Author manuscript of article published in Angewandte Chemie International Edition DOI: 10.1002/anie.202102807

RESEARCH ARTICLE

Thermosensitive vesicles from chemically encoded lipid-grafted elastin-like polypeptides

Vusala Ibrahimova,[a] Hang Zhao,[a] Emmanuel Ibarboure,[a] Elisabeth Garanger,*[a] and Sébastien Lecommandoux*[a]

[a] Dr. V. Ibrahimova, Dr. H. Zhao, E. Ibarboure, Dr. E. Garanger, Prof. Dr. S. Lecommandoux
University of Bordeaux, CNRS,
Bordeaux INP, LCPO, UMR 5629
33600 Pessac (France)
E-mail: garanger@enscbp.fr, sebastien.lecommandoux@u-bordeaux.fr

Abstract: Biomimetic design to afford smart functional biomaterials with exquisite properties represents synthetic challenges and provides unique perspectives. In this context, elastin-like polypeptides (ELPs) recently became highly attractive building blocks in the development of lipoprotein-based membranes. In addition to the bioengineered post-translational modifications of genetically encoded recombinant ELPs developed so far, we report here a simple and versatile method to design biohybrid brush-like lipid-grafted-ELPs using chemical post-modification reactions. We have explored a combination of methionine alkylation and click chemistry to create a new class of hybrid lipoprotein mimics. Our design allowed the formation of biomimetic vesicles with controlled permeability, correlated to the temperature-responsiveness of ELPs.

Introduction

The design of functional membranes mimicking biological materials represents a critical challenge for the study of the origin of life, for artificial cell/protocell construction, biotechnology or pharmaceutical industry.[1,2] Biomimetic models of cellular membranes that can provide an optimal environment to perform multiple complex biochemical reactions (*e.g.*, selective catalytic transformations, complex enzymatic reactions, protein expression, RNA replication) may offer outstanding opportunities for the understanding of cell membrane properties (*e.g.*, endo/exocytosis, cell adhesion, membrane permeation).[1,3-5] Considering the average 60% [6] lipid composition of natural membranes (*i.e.*, cholesterol, phospholipids, glycerophospholipids, sphingolipids, *etc.)*, the first basic synthetic analogues of biological cells reported are 'liposomes' prepared from naturally-occurring phospholipids and composed of a 3-5 nm thick bilayer membrane.[7,8] Later developed 'polymersomes', built from amphiphilic synthetic polymers/polypeptides, provided more mechanically stable vesicle structures owing to macromolecules of higher molar mass and thicker membranes (5-50 nm).[8-11]

Recent advances in cell-mimicking systems have drawn the attention to genetically encoded protein/peptide-based membrane forming bioamphiphiles for potential design of artificial living systems with self-replication, growth and division properties.[6,12-14] Among proteins of interest, elastin-like polypeptides (ELPs) have been proposed as a relevant class of intrinsically disordered proteins (IDPs). ELPs consist in repetitive (-VPG*X*G-) pentapeptide sequences (*X* is a guest residue) and are ideal biomaterials for artificial cells design.[12,13,15,16] ELPs exhibit unique lower critical solution temperature (LCST) phase transition behavior, which drives their transition from a soluble state below their cloud point temperature (T_{cp}) to a dehydrated coacervate state above T_{cp}.[17] In this context, recent synthetic approaches have been proposed to synthesize protein-based amphiphiles as membrane forming materials. Schiller's group introduced genetically encoded amphiphilic proteins built from recombinantly produced and fluorescently labelled diblock elastin-like polypeptides (dbELPs) which formed complex architectures varying from vesicles to twisted fibers upon solvent (*n*-butanol or 1-octanol) assisted self-assembly.[18] Kiick's lab also reported conjugates of elastin-like and collagen-like polypeptides (ELP-CLP) and the production of thermoresponsive, collagen-binding drug delivery vehicles.[19,20] Champion's lab developed another approach to access protein vesicles from ELPs, especially using charge interactions with peptide zippers.[21,22] Francis' lab also reported series of fusion proteins that have been developed to self-assemble spontaneously into stable micelles after enzymatic cleavage of a solubilizing protein tag.[23]

Natural lipidated proteins are reference models for the development of relevant artificial lipid-protein conjugates due to their diverse properties, such as bioactivity, self-assembly and cell membrane anchoring properties that can regulate different cellular functions.[24] In this context, Chilkoti's group has firstly produced post-translationally modified ELPs conjugates with cholesterol [25] and aliphatic myristoyl group [26], exhibiting temperature-triggered self-assembly into a diverse array of structures including fibers, beads-on-a-string coacervates, and networks of fibers. In addition, the production of different derivatives of linear lipid-ELPs *via* post-translational modification, self-assembly into micelles,[27,28] elongated fibers and bottle–brush structures,[29] have also been reported recently by Mozhdehi *et al.* Nevertheless, none of these previous studies using linear lipid-ELP bioamphiphiles have shown or investigated their membrane forming property.

In this work, we have explored a simple and versatile synthetic strategy to chemoselectively graft aliphatic mono-*cis*-unsaturated lipid tails to recombinant ELP [30] backbones to access, for the first time, brush-like biohybrid lipoproteins (Figure 1), that are able to self-assemble into vesicles, also referred to as "lipo-proteinosomes" with a simple solvent free thin film hydration technique.

We hypothesized that this brush-like architecture, where each lipophilic alkyl tail is mimicking the phospholipids' acyl chain, should facilitate vesicle formation stabilized by the peptide backbone which connect 11 lipid tails distributed every 20 probiotic amino acid residues. This novel class of biohybrid amphiphiles combine the best features of the ELP (*e.g.* bioactivity, non-immunogenicity, chemical diversity, multifunctionality and thermal responsiveness) together with the membrane-forming

properties of lipids, enabling the growth of vesicles with temperature responsive on/off release profiles.

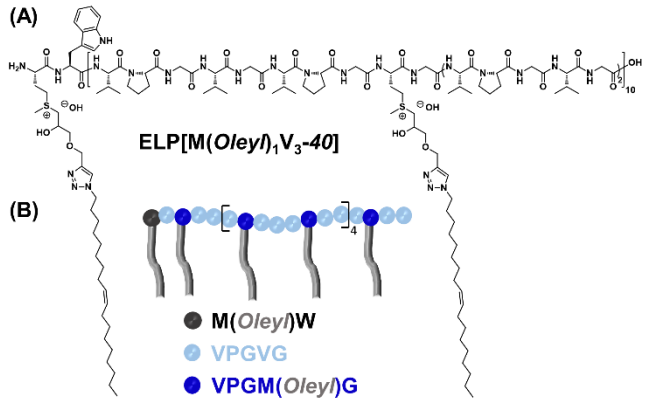

Figure 1. (A) Chemical structure and (B) schematic representation of ELP[M(*Oleyl*)$_1$V$_3$-*40*].

Results and Discussion

Synthesis of lipid-graft-ELP[M$_1$V$_3$-*40*]

The lipoprotein designed in this work is based on a recombinant ELP with the exact protein sequence MW[(VPGVG)(VPGMG)(VPGVG)$_2$]$_{10}$, noted as ELP[M$_1$V$_3$-*40*], produced in *Escherichia coli* bacteria.[31,32] The latter was chemoselectively alkylated using glycidyl propargyl ether to introduce an aliphatic alkyne group on the side chain of the eleven methionine (Met) residues of the ELP as previously reported by our group.[30,31] In parallel, the chlorine group at the chain end of oleyl chloride was converted into an azide group (Scheme S1) for subsequent coupling to ELP[M(*Alkyne*)$_1$V$_3$-*40*] via Huisgen's copper(I)-catalyzed alkyne-azide cycloaddition (CuAAC) reaction. (Scheme S2) Full substitution of the halogen atom by the azide group was confirmed by ^{1}H NMR spectroscopy by the characteristic 0.2 ppm downshifting of α-methylene group's resonance peak from 3.56 to 3.27 ppm, (Figure S1) and by the emerging large -N$_3$ stretching vibration band at 2,092 cm^{-1} in the ATR FT-IR spectrum. (Figure S2) The quantitative grafting of oleyl azide onto ELP[M(*Alkyne*)$_1$V$_3$-*40*] and successful purification of ELP[M(*Oleyl*)$_1$V$_3$-*40*] were confirmed by different techniques namely by ^{1}H NMR spectroscopies, size exclusion chromatography (SEC), SDS-PAGE and ATR FT-IR. (Figures S2-S5)

The ^{1}H NMR spectrum of ELP[M(*Oleyl*)$_1$V$_3$-*40*] showed a well-defined and separated resonance peak at 8.02 ppm corresponding to the newly formed triazole proton which was used as reference to quantify the reaction conversion. (Figure S3) Setting triazole proton peak integral to 11, the expected number of protons for all the well identified and separated peaks were found as indicated in the experimental part. (Table S1)

Comparative SEC chromatograms of the native recombinant ELP[M$_1$V$_3$-*40*] and of ELP[M(*Alkyne*)$_1$V$_3$-*40*] indicated a retarded elution of the latter despite a higher molar mass. This can be attributed to the branching introduced on the polypeptide backbone which significantly affects the hydrodynamic volume of the macromolecule,[33] but also to the positively charged sulfonium groups and associated counterions that may interact with the columns.[30] (Figure S5-A) After grafting of the monounsaturated lipid tail, ELP[M(*Oleyl*)$_1$V$_3$-*40*] displayed a slightly shorter retention time consistent with an increased molar mass. SEC analysis also evidenced a significant peak shoulder attributed to dimer species. The band associated with these dimers was found much weaker in SDS-PAGE analysis which confirmed their non-covalent nature, hydrophobic inter-chain interactions likely occurring between the brush-like lipopeptide chains. (Figure S5-B)

The conjugation was further confirmed by ATR FT-IR spectroscopy following the disappearance of the stretching vibration band of the azide group of the oleyl azide chains and the emergence of new stretching vibration bands at 2,962 and 2,927 cm^{-1} attributed to the asymmetric and symmetric stretching bands of -CH$_2$- [34] indicating a successful lipidation of the ELP. (Figure S2)

The structural characteristics of ELP[M(*Oleyl*)$_1$V$_3$-*40*] are provided in Table 1 and compared to those of synthetic intermediates.

Table 1. Characteristics of ELP derivatives.

Compound	Mn[a]	Đ[a]	MW[b]	Yield[c]	Yield[d]
ELP[M$_1$V$_3$-*40*]	14,930	1.09	17,035	-	-
ELP[M(*Alkyne*)$_1$V$_3$-*40*]	10,270	1.23	18,917	100	91
ELP[M(*Oleyl*)$_1$V$_3$-*40*]	12,520	1.44	23,957	100	64

[a] Number average molar mass (Mn, g.mol^{-1}) and polydispersity index (Đ) were determined by SEC. Dextran used as the standard and dimethysulfoxide (DMSO + lithium bromide LiBr 1 g.L^{-1}) was used as an eluent.
[b] Theoretical molar mass (MW, g.mol^{-1})
[c] Grafting yield determined by ^{1}H NMR (%)
[d] Product yield of reaction (%)

Considering the temperature responsive property of ELP[M$_1$V$_3$-*40*],[32] a monounsaturated aliphatic tail [35] with a low melting transition temperature (T_m = -25 °C, Figure S6) was selected in order to not interfere with the phase transition temperature (T_t) of the ELP. The olefin bond present in natural lipids/fatty acids has a significant impact on the membrane packing and on its fluidity owing to the conformational (*cis*/*trans*) difference.[36] The planar structure, torsion angle and faster rotational motions of the first neighboring single C-C bonds on the *cis* alkyl chains have a significant impact on the formation of well-packed lipid bilayers in natural cell membranes.[36] Whereas the *trans* conformation behaves similar to saturated fatty acids.[36] ATR FT-IR spectroscopy was used to confirm the presence of the characteristic =C-H stretching vibration band of the cis conformation at 3,005 cm^{-1} and the absence of the trans conformation band at 3,034 cm^{-1}.[34] (Figure S2)

Formation of lipo-proteinosomes

The T_{cp} of the final conjugate, ELP[M(*Oleyl*)$_1$V$_3$-*40*], was determined in water (10 mg·mL^{-1}, 417 µM colloidal dispersion) by differential scanning calorimetry (DSC) analysis. (Figure S7) The onset temperature was measured at 25.4 °C on the second heating ramp. This value is very close to the T_{cp} of the unmodified recombinant ELP[M$_1$V$_3$-*40*] (*i.e.*, 22.2 °C, 100 mg·mL^{-1} in water, 5,900 µM), and only slightly lower than the T_{cp} of ELP[M$_1$V$_3$-*40*] at identical molar concentration (417 µM, 30 °C) as expected by turbidimetry assays. (Figure S8) This confirmed that the ELP backbone preserved its thermo-responsiveness after the lipidation. The ELP[M(*Oleyl*)$_1$V$_3$-*40*] dispersion in water was further investigated by dynamic light scattering (DLS) measurements through the scanning of lipopolypeptide solutions in the range of 15-75 °C at 90° angle. (Figure S9-A) The average hydrodynamic diameter of the nanoparticles formed expectedly decreased above 30 °C while the derived count rate increased,

as a consequence of the ELPs dehydration resulting in a conformational change from coils to β-spiral structures above T_{cp} and an increased density of the dispersed particles.[17,37] Additionally, heating-cooling cycles (up to 37 °C and down to 20 °C) confirmed the reversibility of the temperature response, while the size of particles decreased and increased of approximately 45 nm in response to temperature change. (Figure S9-B)

Considering the physico-chemical parameters and phospholipid like structure of Met residues' side chains, we hypothesized that such hybrid brush-like lipoprotein may self-assemble in the aqueous milieu into membrane systems *via* lateral packing of alkyl tails,[38] in a similar manner to natural phospholipids above T_m and be stabilized by the ELP backbone below its T_{cp}. A dense packing of lipid tails may induce the formation of entropically constrained ELP $(VPGVG)_3$ loops in the internal and external surface of the vesicles shell, lipid tails being separated by 20 amino acid residues. To induce the formation of large vesicles, we have chosen the simplest, organic solvent free, conventional vesicle growth technique namely 'thin film hydration' [39] consisting in the formation of a thin lipopolypeptide film on a solid surface that is subsequently swollen by the addition of an aqueous solution to facilitate budding and vesicles growth. (Figure 2-A, experimental section of supporting information (SI))

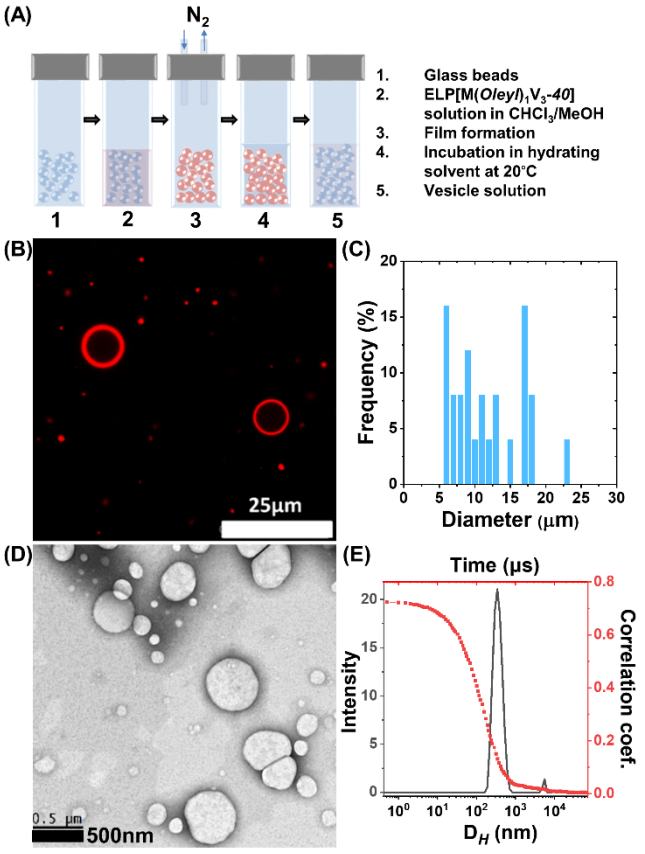

Figure 2. (A) Schematic representation of the glass beads thin film hydration process in water. (B) Confocal laser scanning microscopy image (red channel) of giant lipo-proteinosomes (GLPs obtained using 5 mm beads) at room temperature, and (C) size distribution histogram plotted from the counting of 25 vesicles. (D) Uranyl acetate-stained TEM image of nanometer sized lipo-proteinosomes (NLPs obtained using 0.5 mm beads) with an average size of 295±62 nm (n=20) and (E) 90° angle DLS intensity-averaged distribution of diameters of NLPs at room temperature and correlogram (D_H=372 nm, PDI=0.25).

To increase the surface area of the lipopolypeptide film per volume, provide extra curvatures and have better control on the vesicles growth process, 0.5 and 5 mm size glass beads were used.[40,41] Film hydration on glass beads yields narrow size distribution and allows to reduce the volume of the swelling solvent to microliters thus known as a robust and rapid method.[12,41] Therefore, a thin layer of ELP[M(*Oleyl*)$_1$V$_3$-*40*] lipopolypeptide was formed directly on the surface of the beads by evaporating the solvent via nitrogen flow ($CHCl_3$: MeOH, 8:2). Considering the thermal characteristics of ELP[M(*Oleyl*)$_1$V$_3$-*40*], (Table S2) the film hydration process was conducted in pure deionized water by incubation over 48 h at a temperature below 20 °C. As expected, 5 mm size beads yielded giant lipo-proteinosomes (GLPs), (Figure 2-B, 3 and Figure S9) with micrometer sizes. In contrast, the smaller 0.5 mm beads yielded nanosized lipo-proteinosomes (NLPs) with an average hydrodynamic radius of 372 nm and an estimated membrane thickness of 7.8 nm, consistent with a bilayer packing model. (Figure 2-D, and Figures S11-13) In order to visualize the as-formed vesicles, 5 v% of rhodamine labelled Rhd-ELP[M(*Oleyl*)$_1$V$_3$-*40*] (Scheme S3 and Figure S14) was mixed with the unlabeled lipopolypeptide solution before the film was formed. Images captured by epifluorescence and confocal microscopy confirmed the formation of GLPs with homogeneous membranes as can be seen in Figure 3 and Figure S9 without any defect or domain formation. The use of an excess swelling solvent to cover the large beads yielded a dilute vesicles solution with a broad size distribution varying between 6-23 µm (obtained from confocal images, Figure 2-C). In contrast, the small beads yielded NLPs with an average hydrodynamic radius of 372 nm in good yield and with rather narrow size distributions (PDI=0.25, Figure 2-E) which was in a good agreement with the size obtained from TEM images (295±62 nm, Figure 2-D).

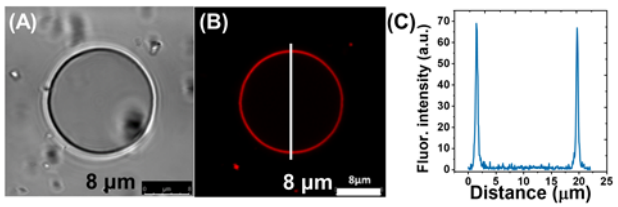

Figure 3. Optical microscopy images of giant lipo-proteinosomes (GLPs) at room temperature. (A) Bright field and (B) red channel images taken with a confocal laser scanning microscope. (C) Fluorescence intensity profile along the white solid line in (B).

Thermo-responsive permeability of lipo-proteinosomes

The vesicles (NLPs) were then subjected to DLS analysis to evaluate the temperature-responsive hydration-dehydration of closely packed ELP chains on the lipoprotein membrane as illustrated in Figure 4-C.

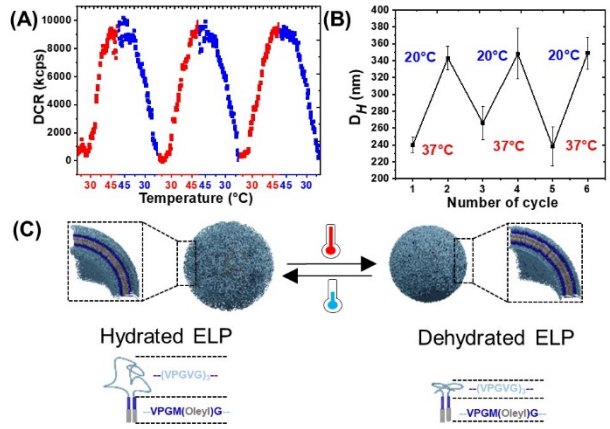

Figure 4. (A) Derived count rate (DCR) versus temperature (20-50 °C) during repetitive heating (red trace) and cooling (blue trace) cycles of NPLs (n=3). (B) Hydrodynamic diameter of NPLs at 20 and 37 °C (average of Z-average (d, nm) size has been used in the figure for each data point, n=3 cycles). (C) Schematic illustration of the thermal responsiveness of NPLs.

Repetitive heating-cooling cycles of NLPs showed an increase in derived count rate as temperature increased above T_{cp} due to the dehydration and collapse of ELP chains, forming a compact vesicle shell. (Figure 4-A) Repetitive heating (n=3) to 37 °C and cooling 20 °C cycles further confirmed the reversibility of the hydration and dehydration process at physiological and room temperatures. (Figure 4-B) After confirming thermo-responsiveness of the ELP[M(*Oleyl*)$_1$V$_3$-*40*] membrane, the effect of temperature on membrane permeability was subsequently evaluated. Self-quenched fluorescein was loaded in NLPs via film hydration in 10 mM fluorescein solution over 48 h. Excess dye was removed by Sephadex G-100 size-exclusion chromatography and the presence of vesicles was confirmed by DLS and TEM measurements. (Figure 5-A)

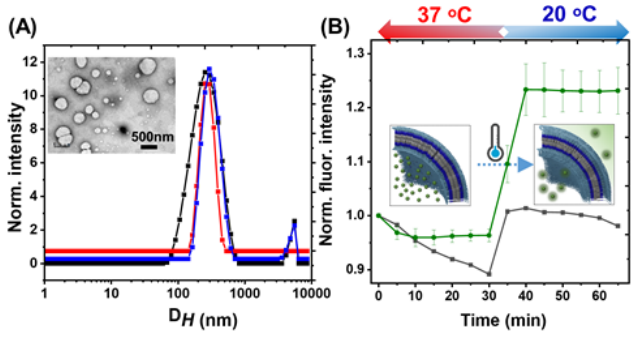

Figure 5. Temperature-triggered dye release from NPLs. (A) DLS intensity-averaged distribution of fluorescein-loaded NLPs (n=3). Insert: characteristic TEM image of NPLs. (B) Fluorescence intensity at 520 nm over time and temperature (n=3) with schematic illustration: NPLs (green trace) and fluorescein in water (black trace).

The NLPs dispersion was immediately placed in the spectrofluorimeter to follow the temperature-responsive on/off dye release profile. The solution was heated above T_{cp} to 37 °C to facilitate the dehydration of the ELP chains that collapsed at the vesicle surface. In these conditions, a constant fluorescence emission of fluorescein at 520 nm (measured every 5 min during 30 min) suggested the stability and impermeability of the NLPs membrane. (Figure 5-B) When temperature was then reduced down to 20 °C (Figure 5-B), a burst release of fluorescein was observed, in correlation with the swelling and decompaction of the ELPs chains. Interestingly, the loading of fluorescein in vesicles also improved the stability of the dye, especially at high temperature (Figure 5-B, grey curve).

.

Conclusion

We reported here a straightforward and versatile design of brush-like ELP[M(*Oleyl*)$_1$V$_3$-*40*] lipopolypeptides allowing the formation of model thermo-responsive membranes with great potential applications in protocell design, nano/micro reactors, drug delivery vehicles with biomimetic character and controlled burst release properties. Such combination of genetically engineered elastin-like polypeptides with chemical post-modification reactions to introduce alkyl chains offers promising opportunities for biohybrid materials design, featuring compartmentalization properties from natural phospholipids combined with temperature responsiveness, bioactivity, sequence-defined structure, reproducibility, easy scalability and narrow molar mass distribution of the genetically engineered and recombinantly produced ELPs.

Acknowledgements

For financial support EuroNanoMed3 TEMPEAT (ANR-17-ENM3-0009) and SIRIC BRIO (INCA, COMMUCAN project) are gratefully acknowledged. Authors wish to thank Bertrand Garbay and Guillaume Goudounet for gene design, cloning and production of ELP[M$_1$V$_3$-*40*]. We gratefully acknowledge Amelie Vax and Anne-Laure Wirotius from LCPO for SEC and NMR analyses, respectively. Continuous support from Univ. Bordeaux, CNRS and Bordeaux-INP is acknowledged.

Keywords: Biomimetic membrane, elastin-like polypeptides, lipoproteins, self-assembly, vesicles.

[1] J. Nam, T. K. Vanderlick, P. A. Beales, *Soft matter* **2012**, *8*, 7982–7988.
[2] T. Ruysschaert, A. F. P. Sonnen, T. Haefele, W. Meier, M. Winterhalter, D. Fournier, *J. Am. Chem. Soc.* **2005**, *127*, 6242–6247.
[3] M. C. Huber, A. Schreiber, S. M. Schiller, *ChemBioChem* **2019**, *20*, 2618–2632.
[4] M. Fiore, P. Strazewski, *Life* **2016**, *6*, 17–35.
[5] S. Ghosh, A. Somasundar, A. Sen, *Annu. Rev. Condens. Matter Phys.* **2021**, *12*.
[6] K. Vogele, T. Pirzer, F. C. Simmel, *ChemSystemsChem* **2019**, *1*, e1900016 (1–7).
[7] A. D. Bangham, M. M. Standish, J. C. Watkins, *J. Mol. Biol* **1965**, *13*, 238–253.
[8] E. Rideau, R. Dimova, P. Schwille, F. R. Wurm, K. Landfester, *Chem. Soc. Rev.* **2018**, *47*, 8572–8610.
[9] X.-Y. Yan, Z. Lin, W. Zhang, H. Xu, Q.-Y. Guo, Y. Liu, J. Luo, X.-Y. Liu, R. Zhang, J. Huang, T. Liu, Z. Su, R. Zhang, S. Zhang, T. Liu, S. Z. D. Cheng, *Angew. Chem. Int. Ed.* **2020**, *59*, 5226–5234.
[10] S. Iqbal, M. Blenner, A. Alexander-Bryant, J. Larsen, *Biomacromolecules* **2020**, *21*, 1327–1350.
[11] H. Che, S. Cao, J. C. M. van Hest, *J. Am. Chem. Soc.* **2018**, *140*, 5356–5359.

[12] K. Vogele, T. Frank, L. Gasser, M. A. Goetzfried, M. W. Hackl, S. A. Sieber, F. C. Simmel, T. Pirzer, *Nat. Commun.* **2018**, *9*, 3862 (1–7).

[13] T. Frank, K. Vogele, A. Dupin, F. C. Simmel, T. Pirzer, *Chem. Eur. J*, **2020**, *26*, 17356–17360.

[14] R. Tan, J. Shin, J. Heo, B. D. Cole, J. Hong, Y. Jang, *Biomacromolecules* **2020**, *21*, 4336–4344.

[15] A. Schreiber, M. C. Huber, S. M. Schiller, *Langmuir* **2019**, *35*, 9593-9610.

[16] H. Zhao, V. Ibrahimova, E. Garanger, S. Lecommandoux, *Angew. Chem. Int. Ed.* **2020**, *59*, 11028–11036.

[17] D. H. T. Le, A. Sugawara-Narutaki, *Mol. Syst. Des. Eng.* **2019**, *4*, 545–565.

[18] A. Schreiber, L. G. Stühn, M. C. Huber, S. E. Geissinger, A. Rao, S. M. Schiller, *Small* **2019**, *15*, 1900163 (1–14).

[19] J. Qin, J. D. Sloppy, K. L. Kiick, *Sci. Adv.* **2020**, *6*, eabd3033 (1–12).

[20] T. Luo, M. A. David, L. C. Dunshee, R. A. Scott, M. A. Urello, C. Price, K. L. Kiick, *Biomacromolecules* **2017**, *18*, 2539–2551.

[21] D. R. Dautel, J. A. Champion, *Biomacromolecules* **2021**, *22*, 116–125.

[22] Y. Jang, M.-C. Hsieh, D. Dautel, S. Guo, M. A. Grover, J. A. Champion, *Biomacromolecules* **2019**, *20*, 3494–3503.

[23] S. H. Klass, M. J. Smith, T. A. Fiala, J. P. Lee, A. O. Omole, B.-G. Han, K. H. Downing, S. Kumar, M. B. Francis, *J. Am. Chem. Soc.* **2019**, *141*, 4291–4299.

[24] M. Takahara, R. Wakabayashi, K. Minamihata, M. Goto, N. Kamiya, *ACS Appl. Bio Mater* **2018**, *1*, 1823–1829.

[25] D. Mozhdehi, K. M. Luginbuhl, M. Dzuricky, S. A. Costa, S. Xiong, F. C. Huang, M. M. Lewis, S. R. Zelenetz, C. D. Colby, A. Chilkoti, *J. Am. Chem. Soc.* **2019**, *141*, 945–951.

[26] D. Mozhdehi, K. M. Luginbuhl, J. R. Simon, M. Dzuricky, R. Berger, H. S. Varol, F. C. Huang, K. L. Buehne, N. R. Mayne, I. Weitzhandler, M. Bonn, S. H. Parekh, A. Chilkoti, *Nat. Chem.* **2018**, *10*, 496–505.

[27] M. S. Hossain, X. Liu, T. I. Maynard, D. Mozhdehi, *Biomacromolecules* **2020**, *21*, 660–669.

[28] D. M. Scheibel, M. S. Hossain, A. L. Smith, C. J. Lynch, D. Mozhdehi, *ACS Macro Lett.* **2020**, *9*, 371–376.

[29] M. S. Hossain, C. Maller, Y. Dai, S. Nangia, D. Mozhdehi, *Chemical Communications* **2020**, *56*, 10281–10284.

[30] M. Rosselin, Y. Xiao, L. Belhomme, S. Lecommandoux, E. Garanger, *ACS Macro Lett.* **2019**, 1648–1653.

[31] R. Petitdemange, E. Garanger, L. Bataille, K. Bathany, B. Garbay, T. J. Deming, S. Lecommandoux, *Bioconjugate Chem.* **2017**, *28*, 1403–1412.

[32] R. Petitdemange, E. Garanger, L. Bataille, W. Dieryck, K. Bathany, B. Garbay, T. J. Deming, S. Lecommandoux, *Biomacromolecules* **2017**, *18*, 544–550.

[33] M. Gaborieau, P. Castignolles, *Anal. Bioanal. Chem.* **2011**, *399*, 1413–1423.

[34] X. Zhang, J. Wei, G. Ren, C. Zhang, Z. Zheng, C. Fan, *Catal. Sci. Technol.* **2019**, *9*, 3380–3387.

[35] G. Wang, Li, S., Lin, H., Brumbaugh, E. E., and Huang, C. h. , *J. Biol. Chem.* **1999**, *274*, 12289–12299.

[36] H.-H. G. Tsai, J.-B. Lee, H.-S. Li, T.-Y. Hou, W.-Y. Chu, P.-C. Shen, Y.-Y. Chen, C.-J. Tan, J.-C. Hu, C.-C. Chiu, *Biochimica et Biophysica Acta (BBA) - Biomembr.* **2015**, *1848*, 1234–1247.

[37] W. Hassouneh, E. B. Zhulina, A. Chilkoti, M. Rubinstein, *Macromolecules* **2015**, *48*, 4183–4195.

[38] J. Jouhet, *Frontiers in Plant Science* **2013**, *4*, 494 (1–5).

[39] H. Zhang, in Liposomes: Methods and Protocols (Ed.: G. G. M. D'Souza), Springer New York, New York, NY, **2017**, 17–22.

[40] K. Vogele, T. Frank, L. Gasser, M. A. Goetzfried, M. W. Hackl, S. A. Sieber, F. C. Simmel, T. Pirzer, *JoVE* **2019**, e59831 (1–8).

[41] A. Wang, A. Ahmad, S. Ullah, L. Cheng, L. Ke, Q. Yuan, *AAPS PharmSciTech* **2017**, *18*, 3227–3235.

RESEARCH ARTICLE

Entry for the Table of Contents

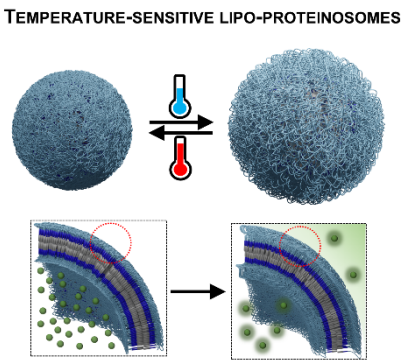

Temperature-sensitive lipo-proteinosomes were engineered by grafting lipids onto temperature-responsive elastin-like polypeptides (ELPs). Maintained at 37°C, folded ELP loops on the internal/external surface of the biohybrid membrane prevents the leaching of encapsulated molecules, while cooling of the dispersion induces a burst release, in correlation with the decompaction of ELP chains.

Institute and/or researcher Twitter usernames: @LCPO_Bordeaux, @LCPO_Poly4Life, @VUSALAIBRAHIMO2, @zhaohang1989, @ElisGaranger, @Biomac_ACS_Bord

Supporting Information

Thermosensitive vesicles from chemically encoded lipid-grafted elastin-like polypeptides

Vusala Ibrahimova, Hang Zhao, Emmanuel Ibarboure, Elisabeth Garanger* and Sébastien Lecommandoux*

Abstract: Biomimetic design to afford smart functional biomaterials with exquisite properties represents synthetic challenges and provides unique perspectives. In this context, elastin-like polypeptides (ELPs) recently became highly attractive building blocks in the development of lipoprotein-based membranes. In addition to the bioengineered post-translational modifications of genetically encoded recombinant ELPs developed so far, we report here a simple and versatile method to design biohybrid brush-like lipid-grafted-ELPs using chemical post-translational modifications. We have explored a combination of methionine alkylation and click chemistry to create a new class of hybrid lipoprotein mimics. Our design allowed the formation of biomimetic vesicles with controlled permeability, correlated to the temperature-responsiveness of ELPs.

DOI: 10.1002/anie.202102807

Table of Contents

Experimental Procedures 3
1. Materials and methods. 3
2. Synthetic procedures 4
2.1 Synthesis of oleyl azide 4
2.2 Synthesis of ELP[M(Oleyl)$_1$V$_3$-40] 5
3. Characterization of the temperature responsive behaver of the ELP[M(*Oleyl*)$_1$V$_3$-4*0*] bioconjugate 8
3.1 Differential scanning calorimetry (DSC) measurement 8
3.2 Dynamic light scattering (DLS) measurement 10
4. Thin film hydration 10
4.1. General procedures for thin film hydration on glass beads. 10
4.2. Fluorescein loading into NPLs 12
5. Fluorescent labeling 13
References 14
Author Contributions 14

Experimental Procedures

1. Materials and methods.

The following reagents were used as received. Copper(II) sulfate pentahydrate ($CuSO_4 \cdot 5H_2O$, 99%) and anhydrous sodium sulfate (Na_2SO_4, 99.5%), sodium azide (NaN_3, 99.5%), sodium sulfate (Na_2SO_4, anhydrous, 99.0%) and 5-Carboxy-X-rhodamine *N*-succinimidyl ester were purchased from Sigma-Aldrich. (+)-sodium L-ascorbate ($C_6H_7NaO_6$, 99%) was obtained from Alfa Aesar. Cis-1-chloro-9-octadecene (oleyl chloride, $C_{18}H_{35}Cl$, 70%) and *N*,*N*-Diisopropylethylamine (DIPEA, 99.0%) were purchased from TCI. Fluorescein disodium salt dehydrate was purchased from Fluka. Cuprisorb® was purchased from Seachem.

The following solvents were used without additional purification: Methanol (MeOH, analytical grade, 100%, VWR chemicals), ethanol (EtOH, absolute, 99.9%, VWR chemicals), *N*-*N*-Dimethylformamide (DMF 99.9%, HPLC grade, VWR chemicals), diethyl ether (Et_2O, 97%, VWR chemicals), dimethyl sulfoxide (DMSO, 99.9%, Sigma-Aldrich) and chloroform ($CHCl_3$, HPLC grade, 99.8%, Sigma-Aldrich). The following deuterated solvents were purchased from Sigma-Aldrich and used without additional purification: Trifluoroacetic acid-d (TFA-d, 99.5 atom % D) and chloroform-d ($CDCl_3$-d, 99.8 atom % D). Ultrapure water (18 MΩ·cm) was obtained by using a Millipore Milli-Q Biocel A10 purification unit.

Spectra/Por Regenerated Cellulose (RC) and Float-A- Lyzer G2 dialysis tubes were used for the purification of ELP-conjugate.

Glass beads (0.5 and 5 mm) were purchased from Sigma-Aldrich.

ELP production: ELP[M_1V_3-*40*] was produced recombinantly in *Escherichia coli* bacteria and purified by *inverse transition cycling* following established procedures.[1-2]

Nuclear Magnetic Resonance (NMR): ^{1}H NMR spectra were recorded with a Bruker AVANCE III HD (Liquid-state 400 MHz NMR spectrometer with 5 mm BBFO probe). Deuterated chloroform ($CDCl_3$, Euriso-top, 99.8%), and deuterated water (D_2O, Euriso-top, 99.8%) were used as solvents and references for the lock. Bruker Topspin Software was used for data treatment.

Size Exclusion Chromatography (SEC): Analyses were performed on an Ultimate 3000 system from Thermoscientific equipped with a diode array detector (DAD). The system from Wyatt technology also includes a multi-angle light scattering detector (MALS) and a differential refractive index detector (dRI). Polypeptide conjugates were separated on two TOSOH successive columns (one G4000PWXL (7.8*300) column with exclusion limits from 2,000 Da to 300,000 Da and one G3000PWXL (7.8*300) column with exclusion limit below 40,000 Da). Analyses were performed at a flow rate of 0.5 mL·min^{-1} and columns temperature was held at 80 °C. Dextran (PSS) was used as the standard. Dimethysulfoxide (DMSO, lithium bromide LiBr 1 g·L^{-1}) was used as eluent and ethylene glycol was used as a flow marker.

Differential scanning calorimetry (DSC): In a dry state, measurement of 10 mg sample was performed using a Q 100-RCS apparatus from TA Instruments over temperature range from -80 to 120 °C, in a heating cooling mode at 5 °C·min^{-1}. The analysis was carried out in a nitrogen atmosphere with aluminum pans.

In a liquid state, measurements were carried out using high pressure crucibles filled with 30 µL of solution sample at a concentration of 10 or 100 mg·mL^{-1} in water. The temperature range was 5 to 50 °C with a heating rate of 2 °C·min^{-1}.

Sodium dodecyl sulfate – polyacrylamide gel electrophoresis (SDS-PAGE) *analysis:* Precision Plus Protein™ Standards (BIO-RAD, unstained) was used as size marker. 20 µL of sample were loaded in gel wells (BIO-RAD, 4–20% Mini-PROTEAN® TGX™ stain-free gel). Tris-Glycine-SDS Buffer (BIO-RAD, TGS 1x) was used as loading buffer. Laemmli Sample Buffer (BIO-RAD, 2x) was used as a running buffer.

Dynamic light scattering measurements (DLS): The measurements were performed on a NanoZS 90 instrument (Malvern, UK) at a 90° angle and at a constant position in the cuvette (constant scattering volume) at different temperatures. The derived count rate (DCR) was defined as the mean scattered intensity normalized by the attenuation factor.

Imaging of giant lipo-proteinosomes: Giant lipo-proteinosomes (GLPs) were collected and imaged in an Ibidi chamber slide (µ-Slide VI 0.4, Ibidi) by using confocal laser scanning microscopy and epifluorescence microscopy. Confocal images were acquired by a confocal laser scanning microscopy (Leica, SP5 AOBS) through an HCX PL APO 63x oil immersion objective. A diode laser (561 nm) was used to excite rhodamine that is labelled on the ELP backbone. Bright field and epifluorescence microscopy images of GLPs were taken on a Zeiss Axiovert 40 CFL inverted microscope with a 100x oil immersion objective captured with a digital Gigabit Ethernet CCD camera (Viewvorks VG-2M). For epifluorescence microscopy, a mercury lamp was used as source with an excitation and emission filter of narrow band pass window in the red for the rhodamine fluorophore (532 to 544 nm for excitation and 573 to 637 nm for emission).

Fluorescence spectrometry: Fluorescence spectra were measured on a JASCO Spectrofluorometer FP-8500 equipped with mini circulation bath (JACOB MCB-100). Light source is 150 W xenon lamp with 1.0 nm wavelength accuracy. The device is equipped with Silicon photodiode (Ex. monochromator) and Photomultiplier (Em. monochromator) detectors. The measurements were taken three times in a 0.5 mL volume quartz cell (2x10 mm light path) and averaged data were used for the final plot.

2. Synthetic procedures

2.1 Synthesis of oleyl azide

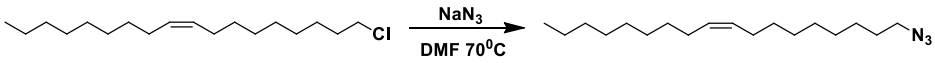

Scheme S1. Synthetic scheme to access oleyl azide from of oleyl chloride.

Oleyl chloride ((Z)-1-chlorooctadec-9-ene, 2 g, 6.97 mmol, 1 equiv.) and sodium azide (2.26 g, 34.8 mmol, 5 equiv.) were dissolved in 10 mL DMF. The reaction mixture was stirred for 24 h at 70 °C and then diluted with 100 mL petroleum ether. The organic phase was washed twice with ultrapure water (50 mL) and then dried over anhydrous sodium sulfate (Na_2SO_4). After filtration and removal of the organic solvent under vacuum, oleyl azide was isolated as a transparent oily liquid (1.96 g, 6.68 mmol) with quantitative conversion yield (100%).
^{1}H NMR (400 MHz, $CDCl_3$): δ 5.38- 5.36 (m, 2H, =C*H*-), 3.29–3.25 (t, 2H, αCH_2), 2.05-1.99 (m, 4H, =CH-CH_2-), 1.65-1.58 (m, 2H, βC*H*), 1.33-1.29 (m, 22H, CH_2), 0.93–0.89 (t, 3H, -CH_3). ATR FT-IR υ_{max} 3005, 2922, 2853, 2092, 1463, 1348, 1258, 986, 897, 722, 557 cm^{-1}. Product yield: 96%.

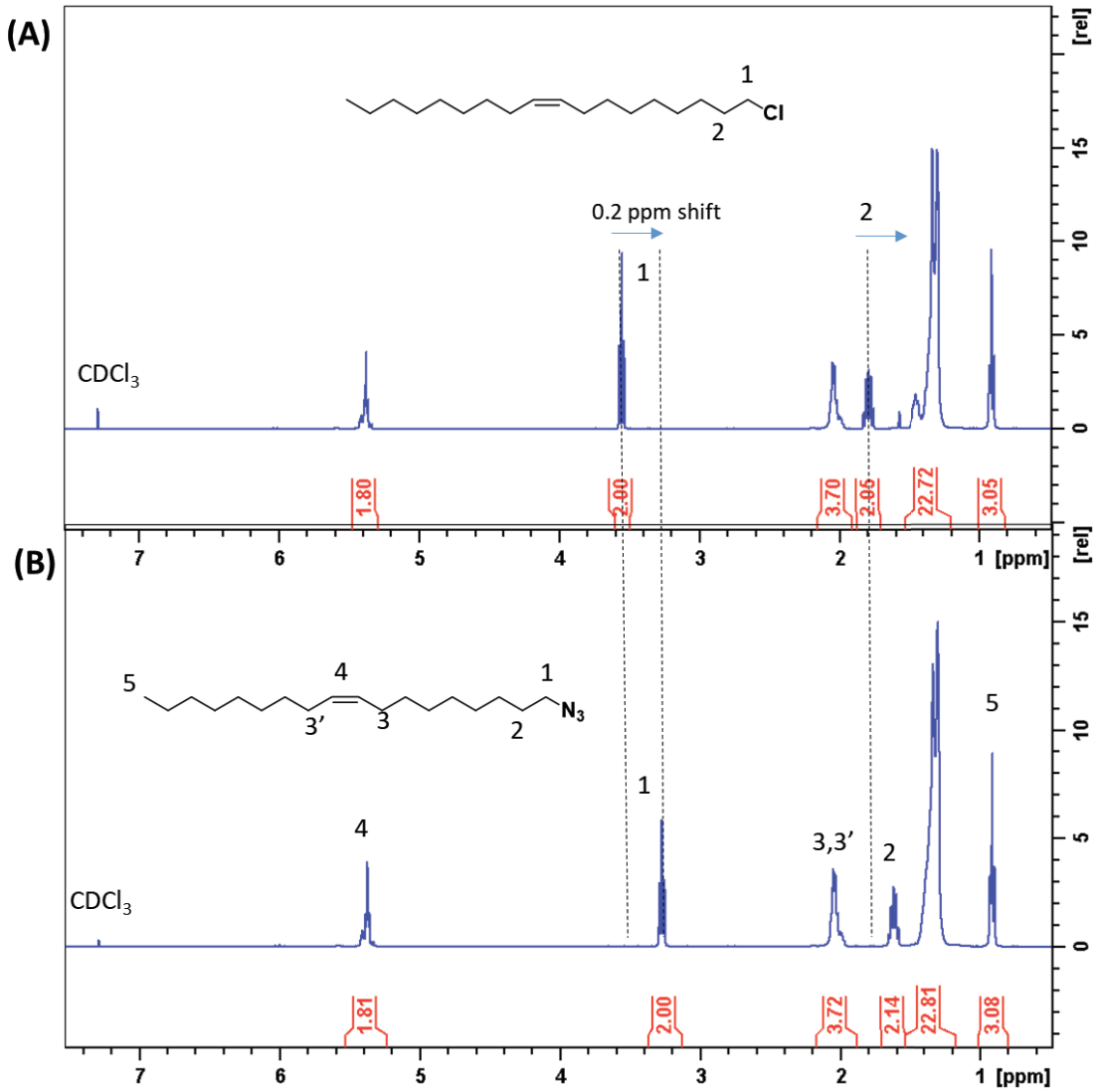

Figure S1. ^{1}H NMR spectra of commercial oleyl chloride (A) and oleyl azide (B) in $CDCl_3$ at room temperature (peak 1- used for the calibration).

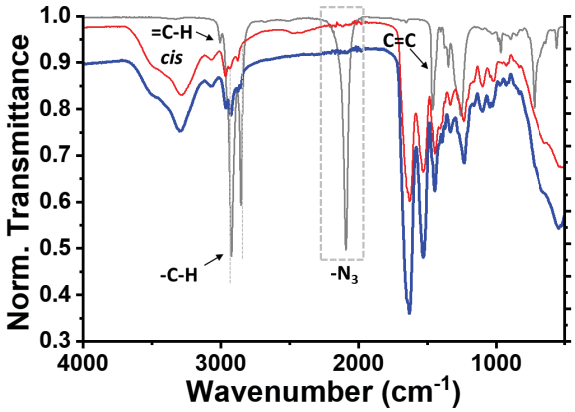

Figure S2. ATR FT-IR transmittance spectra of oleyl azide (grey), ELP[M(*Alkyne*)$_1$V$_3$-*40*] (red) and ELP[M(*Oleyl*)$_1$V$_3$-*40*] (blue)

2.2 Synthesis of ELP[M(Oleyl)$_1$V$_3$-40]

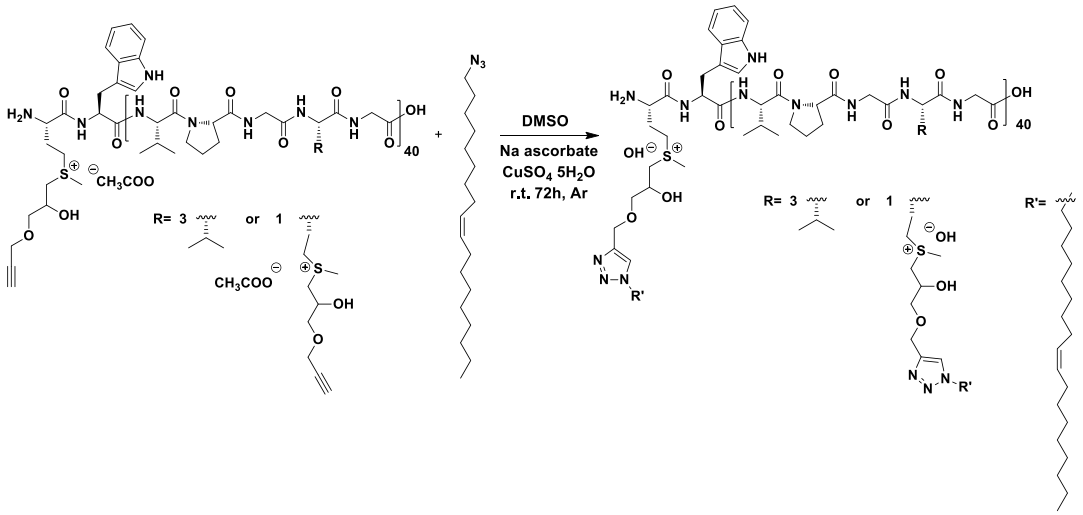

Scheme S2. Synthetic scheme of the Huisgen's copper (I)-catalyzed alkyne-azide cycloaddition (CuAAC) reaction between ELP[M(*Alkyne*)$_1$V$_3$-*40*] and oleyl azide yielding the lipopolypeptide ELP[M(*Oleyl*)$_1$V$_3$-*40*].

ELP[M(*Alkyne*)$_1$V$_3$-*40*] [3],[4] (60 mg, 3.17 µmol, 1 equiv.), oleyl azide (23 mg, 79.29 µmol, 25 equiv.), copper sulfate $CuSO_4 \cdot 5H_2O$ (1 mg, 3.17 µmol, 3 equiv.) and sodium ascorbate (1 mg, 6.34 µmol, 3.5 equiv.) were dissolved in 3 mL anhydrous DMSO and the solution was immediately degassed by freeze-thaw-freeze cycles. The reaction mixture was stirred for 72 h at ambient temperature under argon. Excess copper was removed using Cuprisorb beads and subsequent filtration. The reaction product was precipitated twice with cold diethyl ether. The precipitate was centrifuged for 50 min at 15 °C (3,800 RPM). The supernatant was discarded and the pellet was dissolved in methanol and dialyzed extensively against ultrapure water using dialysis tubing (10 kDa MWCO) for 48 h to remove the excess sodium ascorbate. The final solution was lyophilized to obtain 47 mg (2.12 µmol) ELP[M(*Oleyl*)$_1$V$_3$-*40*] as a white powder. ^{1}H NMR (400 MHz, 15% TFA-d in $CDCl_3$): (main peaks) δ=8.02 ppm (s, 11H, triazole *H*), 5.25–5.22 (t, 22H, -*H*C=C*H*- Ole), 4.27 (br d, 33H, αC*H* Met), 2.85-2.82 (m, 33H, -SCH_3), 1.16 (d, 30H, βC*H* Val; 308H, -CH_2- Ole), 0.85–0.79 (m, -CH_3 Val, -CH_3 Ole). ATR FT-IR υ_{max} 3299, 3073, 2962, 2927, 1632, 1531, 1446, 1392, 1233, 1100, 1047, 928, 541 cm^{-1}. SEC: Mw 12,520 Da, Đ =1.44. Yield: 67%.

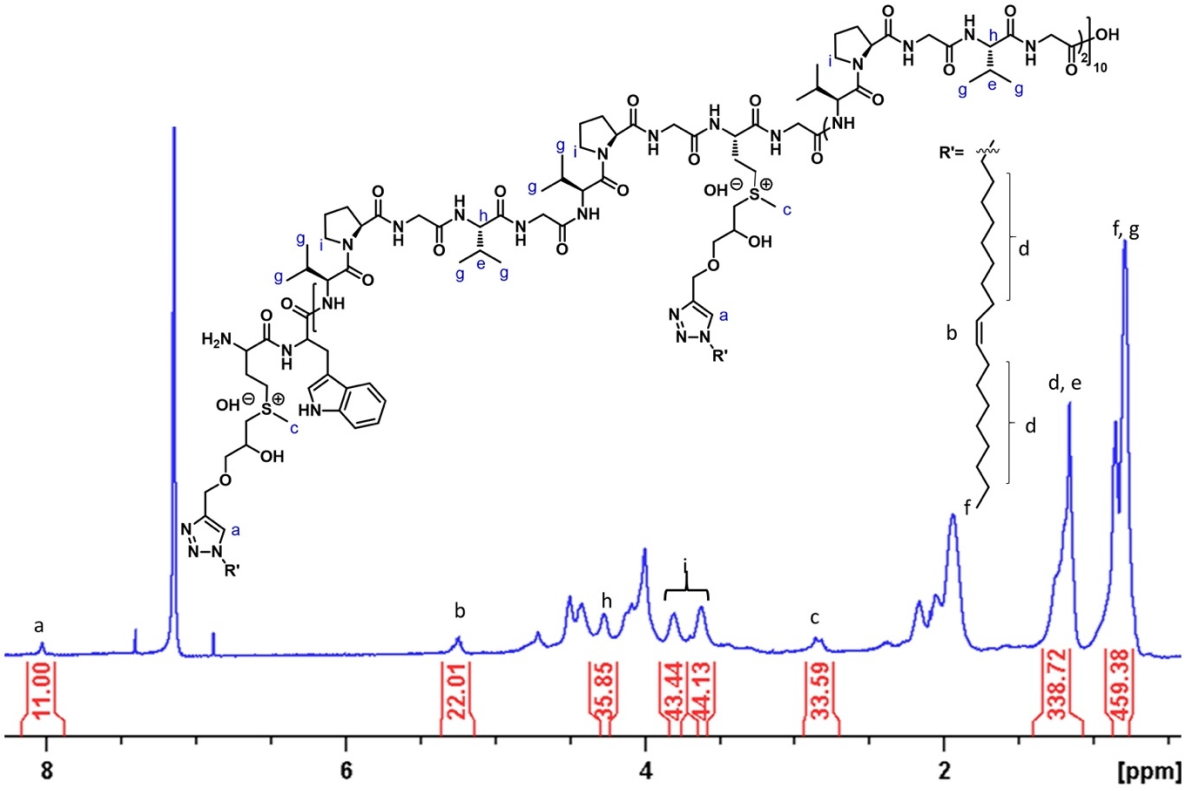

Figure S3. ^{1}H NMR spectrum of ELP[M(*Oleyl*)$_1$V$_3$-*40*] in $CDCl_3$ (15% TFA-d) at room temperature.

Table S1. ^{1}H NMR spectrum characterization of ELP[M(*Oleyl*)$_1$V$_3$-*40*]

Proton	Theoretical	Experimental	Comment
a	11 H	11 H	Peak used as reference
b	22 H	22 H	Olefin bond protons
c	33 H	33 H	
d	308 H	338 H	Overlapped with e
e	30 H		Overlapped with d
f	33 H	459 H	Overlapped with g
g	420 H		Overlapped with f
h	30 H	35 H	
i	80 H	87 H	

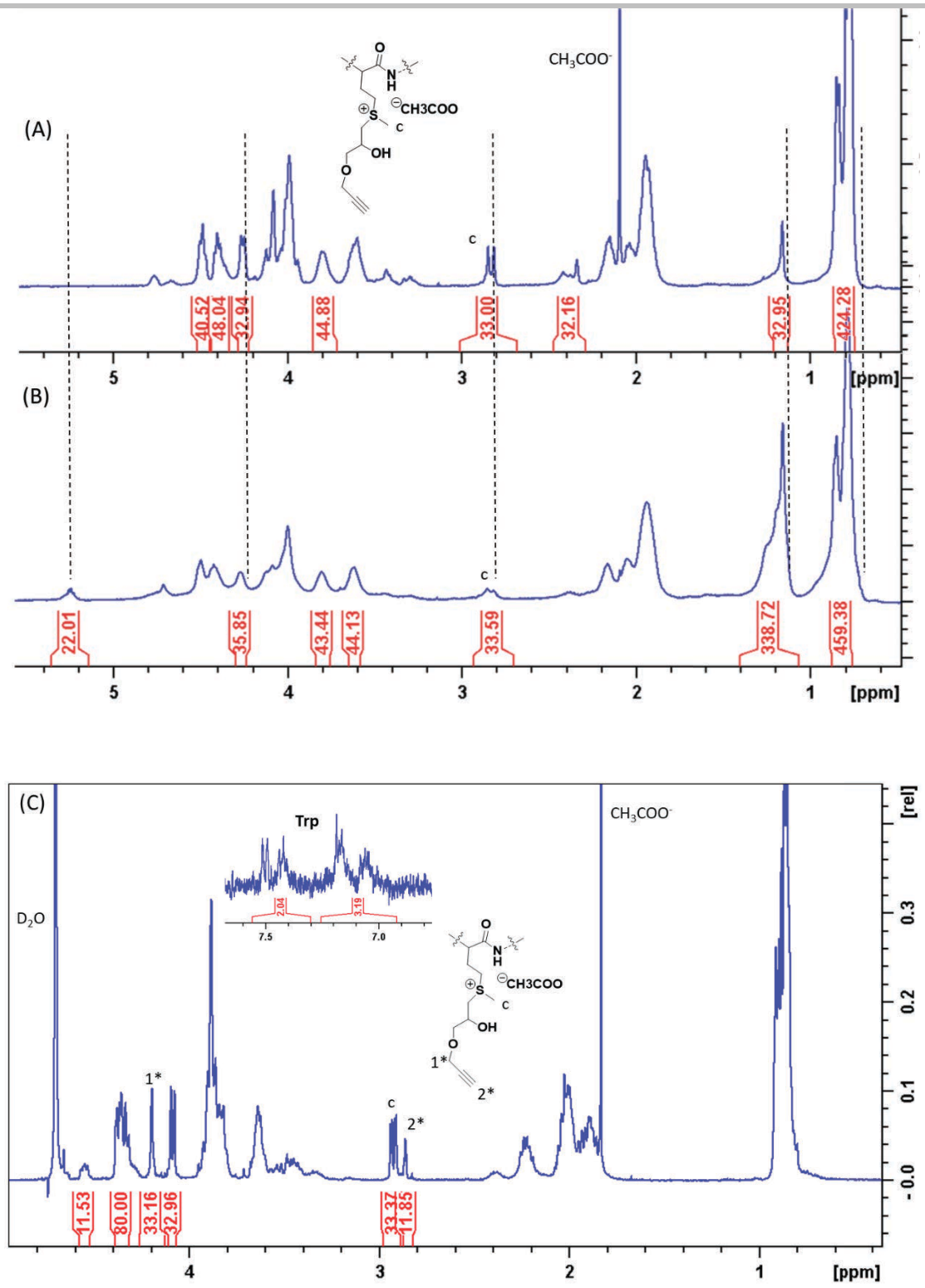

Figure S4. ^{1}H NMR spectrum of (A) ELP[M(*Alkyne*)$_1$V$_3$-*40*] and (B) ELP[M(*Oleyl*)$_1$V$_3$-*40*] in $CDCl_3$ (15% TFA-d) and (C) ELP[M(*Alkyne*)$_1$V$_3$-*40*] (data provided only serve for comparison with the new product claimed) [3],[4] in D_2O at room temperature.

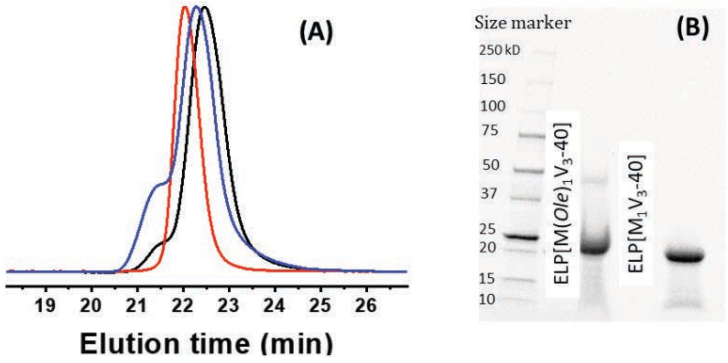

Figure S5. Normalized SEC chromatograms of ELP[M_1V_3-*40*] (red), ELP[M(*Alkyne*)$_1V_3$-*40*] (black) and ELP[M(*Oleyl*)$_1V_3$-*40*] (blue) in DMSO and (B) SDS-PAGE analysis.

3. Characterization of the temperature responsive behaver of the ELP[M(*Oleyl*)$_1$V$_3$-*40]* bioconjugate

3.1 Differential scanning calorimetry (DSC) measurement

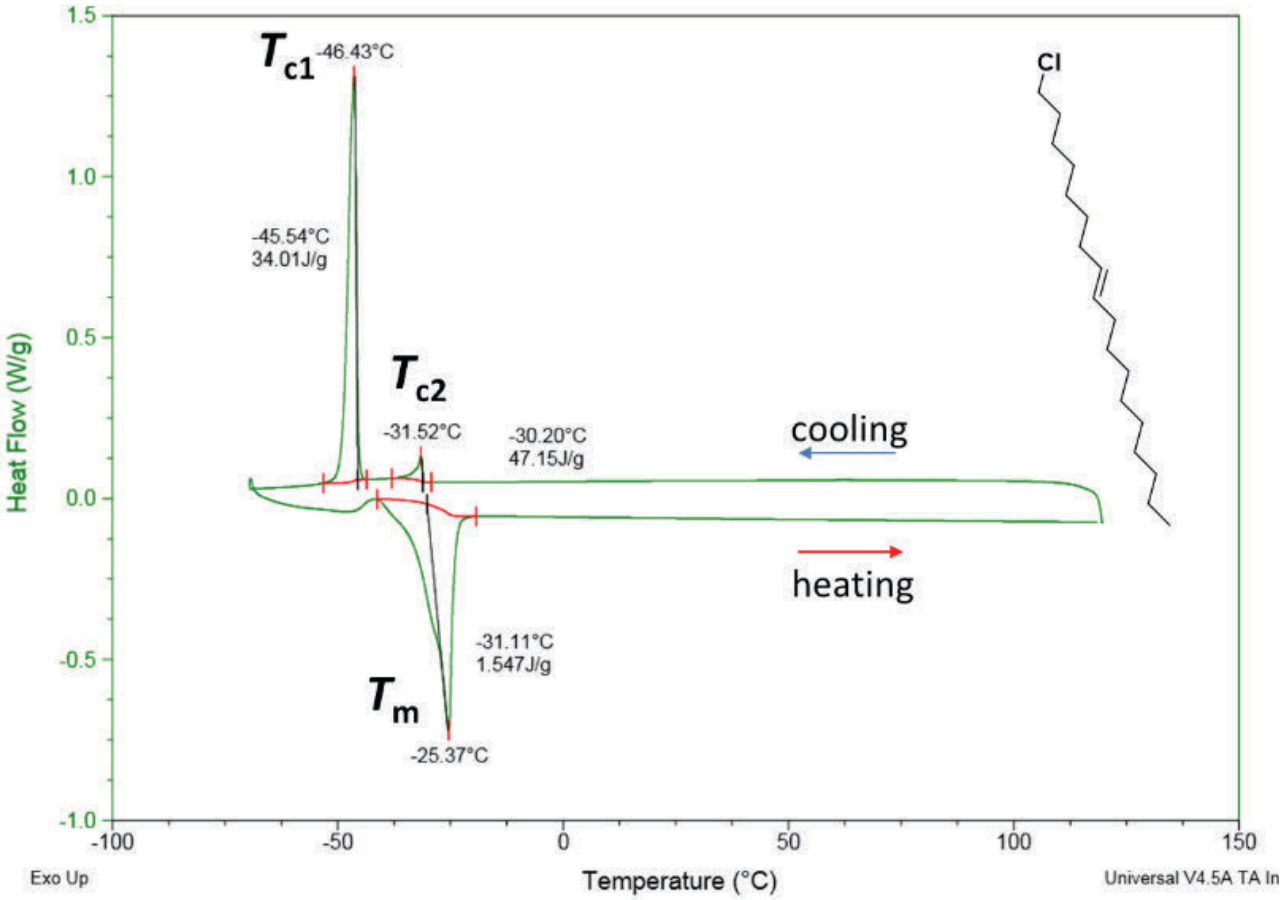

Figure S6. DSC thermogram of commercial oleyl chloride cooling run and second heating run.

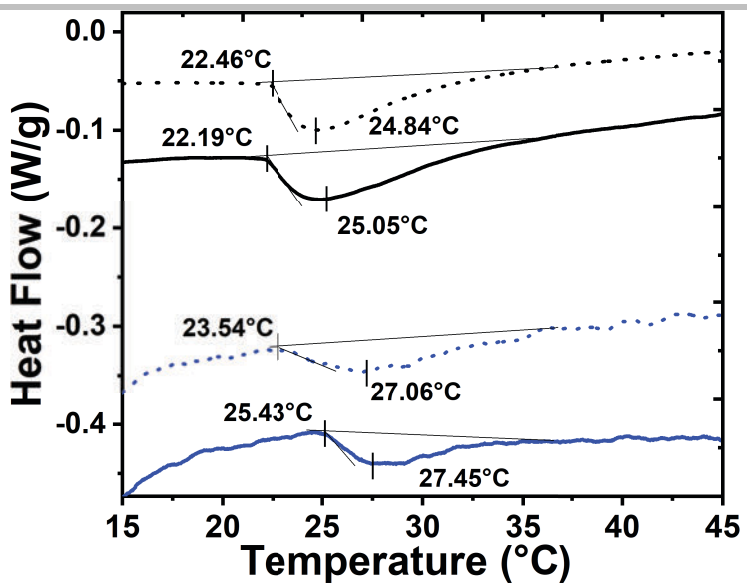

Figure S7. DSC thermograms of 100 mg mL^{-1} ELP[M_1V_3-*40*] (5,900 μM) in water (black dash line first heating and black solid line second heating run) and 10 mg mL^{-1} ELP[M(*Oleyl*)$_1$$V_3$-*40*] dispersion in water (417 μM) (blue dash line first heating and blue solid line second heating run)

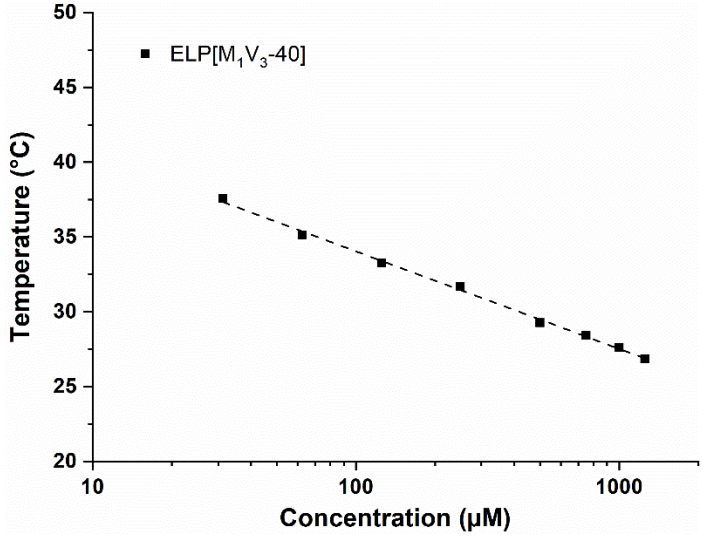

Figure S8. T_{CP} (°C) of ELP[M_1V_3-*40*] versus molar concentration in water as measured by turbidimetry.[5] Following the empirical model established by Chilkoti et al.,[6] the equation of the fitted line is T_{CP} = -2.83 ln(C) + 47.08.

Table S2. Summary of the DSC characterization results

Name	T_{cp} (°C)	T_m (°C)	T_c (°C)
Oleyl chloride		-25	-31, -46
ELP[M_1V_3-*40*]	25		
ELP[M(*Oleyl*)$_1$$V_3$-*40*]	27		

T_{cp} cloud point temperature, T_m melting transition temperature and T_c crystallization temperature determined by DSC respectively from second heating run

3.2 Dynamic light scattering (DLS) measurement

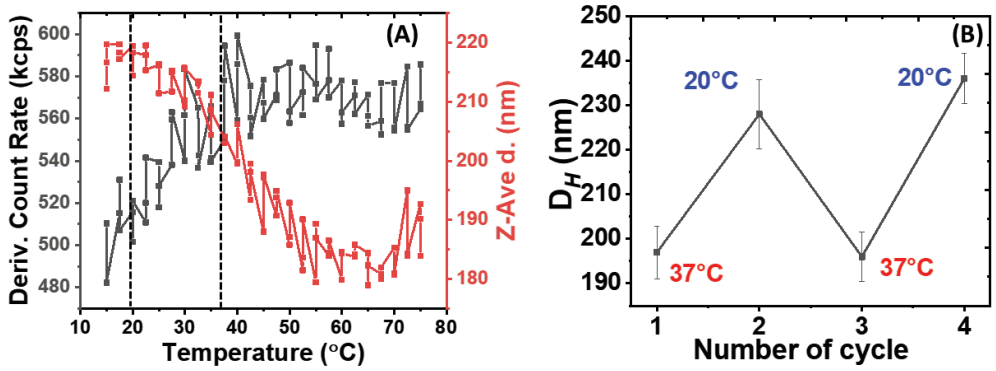

Figure S9. Dynamic light scattering results of 10 mg·mL^{-1} ELP[M(*Oleyl*)$_1$V$_3$-*40*] dispersion in water (A) heating scan from 15 to 75 °C (at each temperature n=3 scans have been performed) and (B) repetitive heating-cooling cycle above and below the T_{cp} (average of Z-average (d, nm) size has been used in the figure for each data point for n=3 measurements).

Preparation of ELP[M(Oleyl)$_1$V$_3$-40] dispersion in water: 10 mg of ELP[M(*Oleyl*)$_1$V$_3$-*40*] dissolved in 0.5 mL of MeOH at 40 °C and diluted with 0.5 mL of water at room temperature. The dispersion was transferred to Float-A- Lyzer G2 dialysis tube (MWCO 100 kDa, 1 mL) and dialyzed for 48 h in ultrapure water to remove MeOH and obtain ELP[M(*Oleyl*)$_1$V$_3$-*40*] dispersion in water.

4. Thin film hydration

4.1. General procedures for thin film hydration on glass beads.

Stock solutions at 1 mg·mL^{-1} ELP[M(*Oleyl*)$_1$V$_3$-*40*] and Rhd-ELP[M(*Oleyl*)$_1$V$_3$-*40*] in $CHCl_3$:MeOH (8:2) were prepared.

0.5 mm glass beads: 100 µL ELP[M(*Oleyl*)$_1$V$_3$-*40*] solution was added onto 400 mg of the beads in a vial. The solvent was evaporated under nitrogen flow while gentle hand shaking until the bioamphiphile film was formed on the surface of the beads. To remove traces of solvent, the vial was kept under vacuum overnight. 200 µL of the swelling solvent (ultrapure water) was then added onto the beads and incubated for 48 h at a temperature below 20 °C. The NLPs solution was collected by decantation.

5 mm glass beads: 5 g of beads were added into a round-bottom flask and 200 µL ELP[M(*Oleyl*)$_1$V$_3$-*40*] solution (mixed with 5% Rhd-ELP[M(*Oleyl*)$_1$V$_3$-*40*]) was added. The solvent was evaporated under nitrogen flow while gentle hand shaking until the bioamphiphile film was formed on the surface of the beads. To remove traces of solvent, the round-bottom flask was been kept under vacuum overnight. 2 mL of the swelling solvent (ultrapure water) was then added onto the beads and incubated for 48 h at a temperature below 20 °C. The GLPs solution was collected by decantation.

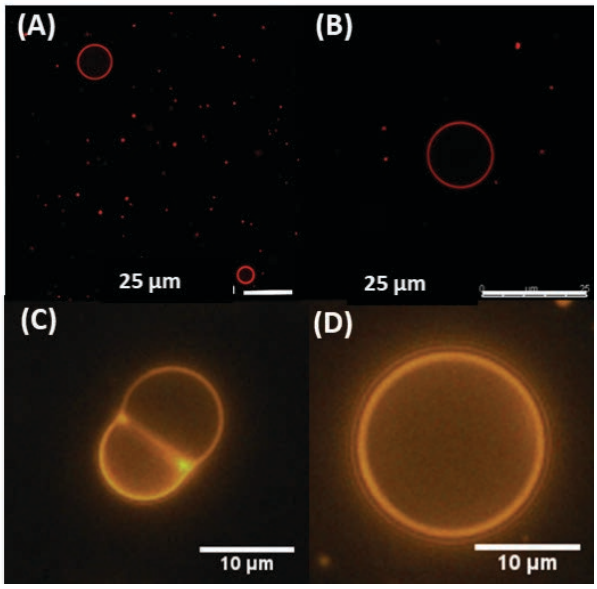

Figure S10. Optical microscopy images of giant lipo-proteinosomes (GLPs) at room temperature. (A) and (B) red channel images taken with a confocal laser scanning microscope. (C) and (B) rhodamine filter set images taken with an epifluorescence microscope.

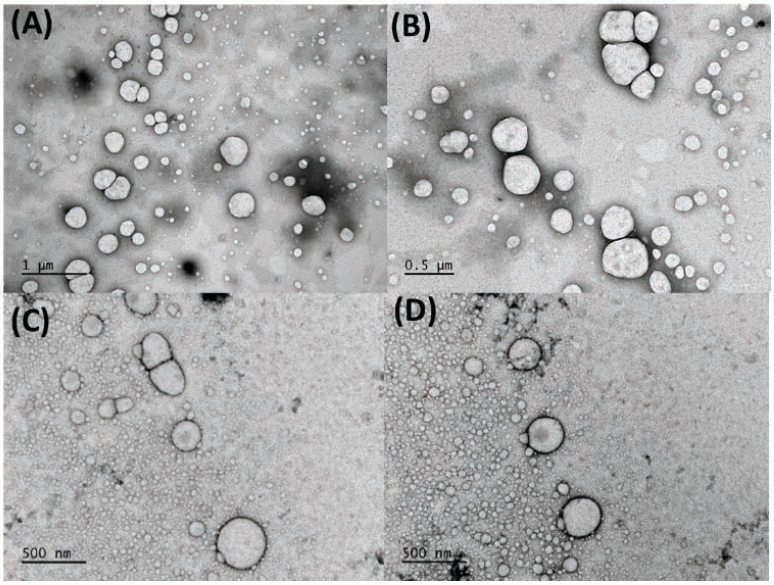

Figure S11. Uranyl acetate-stained TEM images of nanometer sized lipo-proteinosomes (NLPs obtained using 0.5 mm beads). (A) and (B) freshly prepared sample. (C) and (D) one week old samples that kept at room temperature.

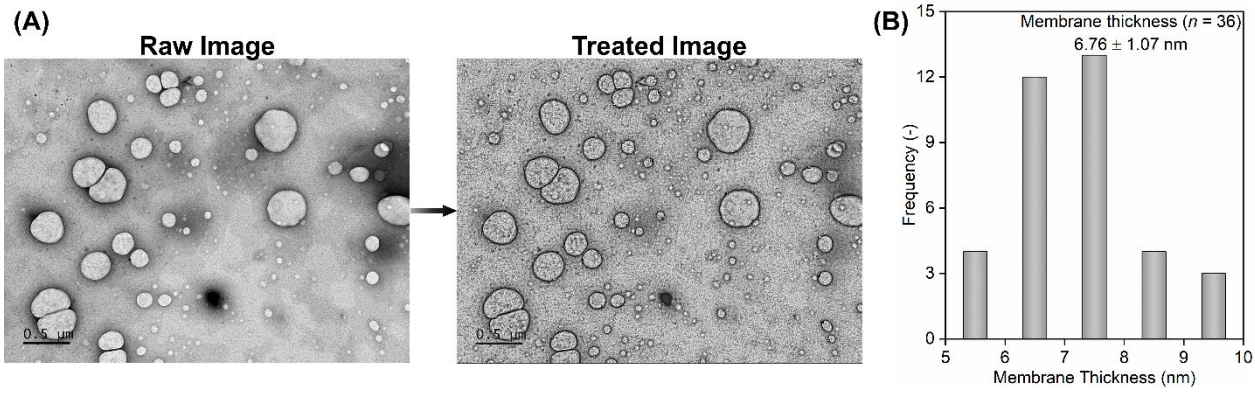

Figure S12. (A) Treatment of the TEM image for measurement of bilayer thickness in ImageJ. (B) Histogram of the membrane thickness of nanosized lipo-proteinosomes.

Membrane thickness was measured from TEM images. To obtain a higher contrast between stained membranes and background, the TEM image was treated with the ImageJ software where subtraction of background (rolling ball radius 500 pixels) was first employed, then local contrast was enhanced (blocksize 50; histogram bins 256; maximum slope 3). (Figure S12 (A)) In total, 36 vesicular structures were analyzed and the average thickness of membranes could be estimated to 6.76 ± 1.07 nm. (Figure S12 (B))

Due to the staining method for the TEM imaging (negative contrast), this membrane thickness is likely to include all the ELP[M(*Oleyl*)$_1$V$_3$-*40*] lipoprotein size. To validate the membrane thickness measured from the TEM analysis, we proposed a model resulting from the self-assembly of our lipo-polypeptides (Figure S13).

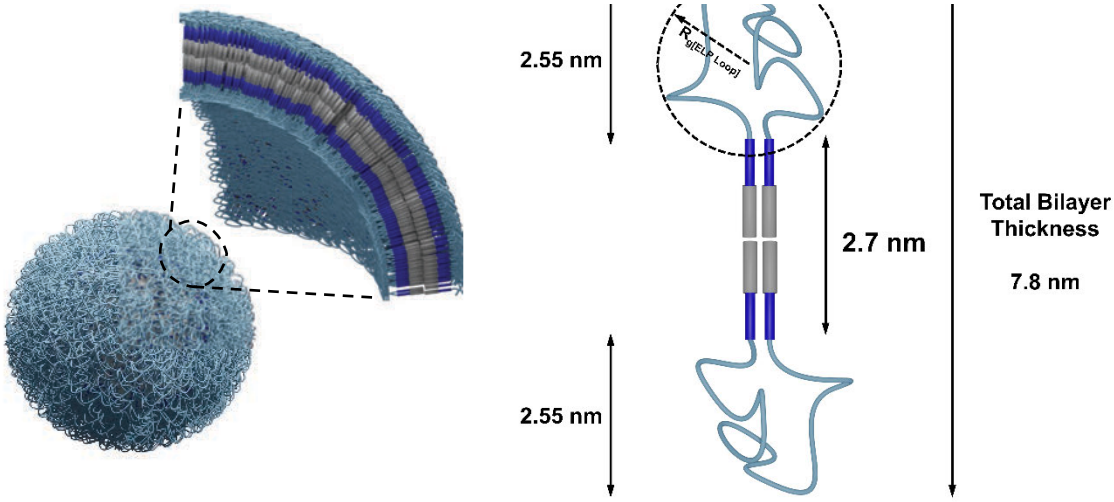

Figure S13. Scheme of one assembling unit of lipo-proteinosome membrane and schematic illustration of the membrane thickness.

One can first anticipate that the oleyl aliphatic mono-*cis*-unsaturated lipid tail used in the present study shares similar structure with the hydrophobic tail of 1-palmitoyl-2-oleoyl-glycero-3-phosphocholine (**POPC**) whose thickness of the tail domain is reported to be 2.7 nm.[7] Thus the hydrophobic thickness of self-assembled lipo-proteinosome membranes will be the same as 2.7 nm. In a previously reported article,[8] we have established a scaling law to determine the radii of gyration ($\mathbf{R_g}$) of hydrated diblock ELPs (namely below their T_{cp}) as a function of their molecular weight ($\mathbf{M_w}$).

$$R_g = 0.505 \cdot M_w^{0.486}$$

We adopt this scaling law to first calculate the $\mathbf{R_g}$ of the ELP fraction that is separated by two individual lipid tails. As demonstrated in the manuscript, 20 amino acid residues are aligned in between two neighbouring lipid tails, which contribute one tenth of total molecular weight of the ELP backbone (17000 g mol^{-1}). Therefore, the molecular weight of the ELP fragment is 1700 g mol^{-1}. According to the scaling law, we are able to calculate the $\mathbf{R_g}$ corresponding to this fragment of chain:

$$R_g = 0.505 \cdot 1700^{0.486} = 18.8\ \text{Å} = 1.9\ \text{nm}$$

However, when vesicles are formed, the ELP fraction is exposed to the aqueous medium forming a loop conformation at this interface rather than a linear extended one (Figure S13). One would thus assume this ELP loop $\mathbf{R_g}$ to be estimated as a cyclic. Borsali *et al*. has reported that the radius of gyration of a cyclic polymer in solution can be determined from its linear counterpart from the following equation:[9]

$$R_{gl} = \sqrt{2} \cdot R_{gr}$$

Where the subscripts **l** and **r** refer to linear and ring polymers, respectively. The radius of gyration of the ELP loop ($\mathbf{R_{g[ELP\ Loop]}}$) can thus be estimated:

$$R_{g[ELP\ Loop]} = 1/\sqrt{2}\ .\ R_{gl} = 1.27\ \text{nm}$$

Finally, we could estimate the total bilayer thickness of our lipo-proteinosomes that is 7.8 nm, which is consistent with our measurements from TEM image. These results strongly suggest that the packing model proposed resulting from the self-assembly of our lipopolypeptides into vesicular structure, seem realistic.

4.2. Fluorescein loading into NPLs

The film hydration on 0.5 mm size glass beads was repeated using 10 mM fluorescein disodium salt dehydrate solution in water as hydrating solvent. After 48 h incubation at a temperature below 20 °C, the mixture was loaded into 20 mL of pre-prepared Sephadex G-100 column (13 mm diameter, 25 cm height) to eliminate unloaded fluorescein. The dispersion was immediately analyzed by DLS and fluorescence spectrometry. To prevent the dye release before the analysis, the temperature of the dispersion was kept above the T_{cp}.

5. Fluorescent labeling

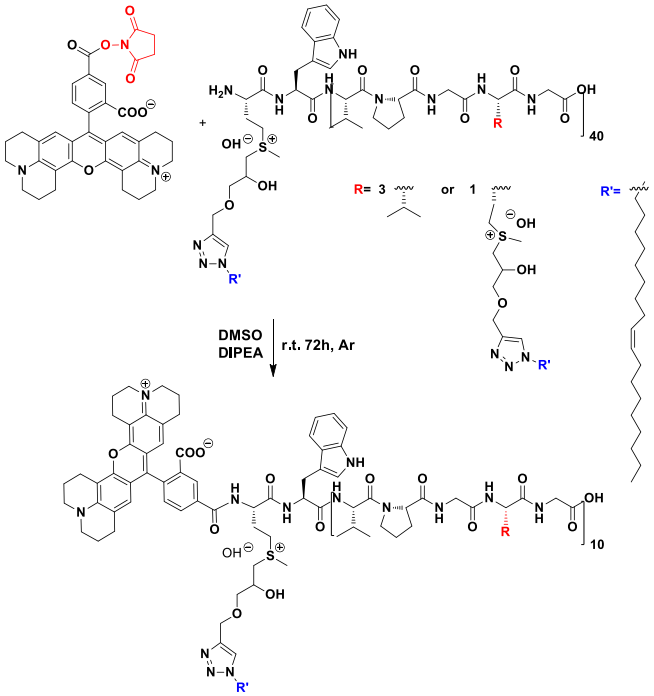

Scheme S3. N-terminus labelling of ELP[M(*Oleyl*)$_1$V$_3$-*40*] by rhodamine-NHS ester in DMSO.

To a solution of ELP[M(*Ole*)$_1$V$_3$-*40*] (10 mg, 41.7 10 µmol) in anhydrous DMSO (1 mL) was added DIPEA (0.07 µL, 41.7 10 µmol). After stirring the solution rhodamine-NHS ester (5-carboxy-X-rhodamine *N*-succinimidyl ester, 0.3 mg, 41.7 10 µmol) was added and the reaction was left under stirring for 72 h at room temperature in the dark under N_2. Then the mixture was precipitated into diethyl ether: EtOH (9:1) 3x times. The precipitate was dissolved in 2 mL MeOH and diluted with water (10 mL) placed in dialysis bag (15 kDa cut off) and dialyzed against water for 3 days in the dark (change the water 3 times per day). The final pale pink product Rhd-ELP[M(*Oleyl*)$_1$V$_3$-*40*] was obtained by lyophilization. (6 mg, 60% product yield)

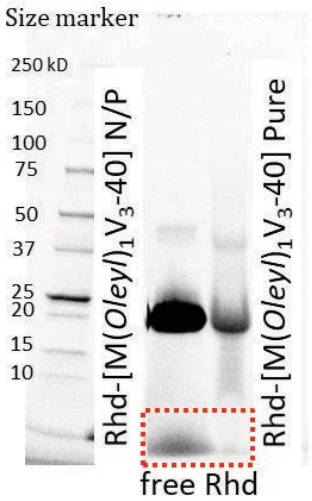

Figure S14. SDS-PAGE analysis before (N/P- non-purified) and after the removal of free rhodamine dye.

References

[1] Meyer, D. E.; Chilkoti, A., Genetically Encoded Synthesis of Protein-Based Polymers with Precisely Specified Molecular Weight and Sequence by Recursive Directional Ligation: Examples from the Elastin-like Polypeptide System. *Biomacromolecules* **2002**, *3*, 357-367.

[2] Petitdemange, R.; Garanger, E.; Bataille, L.; Bathany, K.; Garbay, B.; Deming, T. J.; Lecommandoux, S., Tuning Thermoresponsive Properties of Cationic Elastin-like Polypeptides by Varying Counterions and Side-Chains. *Bioconjugate Chemistry* **2017**, *28*, 1403-1412.

[3] Kramer, J. R.; Petitdemange, R.; Bataille, L.; Bathany, K.; Wirotius, A.-L.; Garbay, B.; Deming, T. J.; Garanger, E.; Lecommandoux, S., Quantitative Side-Chain Modifications of Methionine-Containing Elastin-Like Polypeptides as a Versatile Tool to Tune Their Properties. *ACS Macro Letters* **2015**, *4*, 1283-1286.

[4] Rosselin, M.; Xiao, Y.; Belhomme, L.; Lecommandoux, S.; Garanger, E., Expanding the Toolbox of Chemoselective Modifications of Protein-Like Polymers at Methionine Residues. *ACS Macro Letters* **2019**, 1648-1653.

[5] Xiao, Y.; Chinoy, Z. S.; Pecastaings, G.; Bathany, K.; Garanger, E.; Lecommandoux, S., Design of Polysaccharide-b-Elastin-Like Polypeptide Bioconjugates and Their Thermoresponsive Self-Assembly. *Biomacromolecules* **2020**, *21*, 114-125.

[6] McDaniel, J. R.; Radford, D. C.; Chilkoti, A., A Unified Model for De Novo Design of Elastin-like Polypeptides with Tunable Inverse Transition Temperatures. *Biomacromolecules* **2013**, *14*, 2866-2872..

[7] Ellena, J. F.; Lackowicz, P.; Mongomery, H.; Cafiso, D. S., Membrane Thickness Varies Around the Circumference of the Transmembrane Protein BtuB. *Biophysical Journal* **2011**, *100* (5), 1280-1287.

[8] Garanger, E.; MacEwan, S. R.; Sandre, O.; Brulet, A.; Bataille, L.; Chilkoti, A.; Lecommandoux, S., Structural Evolution of a Stimulus-Responsive Diblock Polypeptide Micelle by Temperature Tunable Compaction of its Core. *Macromolecules* **2015**, *48* (18), 6617-6627.

[9] Borsali, R.; Benmouna, M., Static Scattering from Cyclic Copolymers in Solution. *Macromolecular Symposia* **1994**, *79*, 153-166.

Author Contributions

The manuscript was written through contributions of all authors. / All authors have given approval to the final version of the manuscript.

Funding Sources: Euronanomed III TEMPEAT projet (ANR-17-ENM3-0009) and SIRIC BRIO (INCA, COMMUCAN project) are gratefully acknowledged for financial support.

Notes: The authors declare no competing financial interest.